Ultra-Wideband-based Trajectory Estimation Algorithm with Adaptive Square Root Cubature Kalman Filtering

Wu QingYi [1, 2,*], Liu Zhong [1], Zhang JianQiang [1] and Sun KaiWen [3]

[1]*College of Electronic Engineering, Naval University of Engineering, Wuhan 430000, China*
[2] *College of naval aviation, Huludao 125000, China*
[3]*Department of Computer Science and Engineering, University of California, San Diego, CA 92093, United States*

___

Abstract

The accurate and real-time performance of trajectory estimation directly affects projectile observation and correction. However, estimation performance may suffer from poor real-time and weak anti-jamming capabilities when sensors, such as optics/acoustics, global positioning system, or radar are used to estimate trajectory. This study proposed a novel trajectory estimation algorithm based on the ultra-wideband (UWB) positioning technique to improve real-time estimation accuracy. The state equation was established based on UWB positioning technology, which combined time difference of arrival (TDOA) and angle of arrival, and then compared with single TDOA location technology. Square root cubature Kalman filter (SRCKF) was used to estimate the trajectory. However, the filtering accuracy decreased when the measured value was abnormal. The adaptive square root cubature Kalman filter (ASRCKF) method was proposed to deal with this problem. Judgment as to whether the ASRCKF method should be used was presented. Results show that the joint positioning method is superior to the single positioning method, and that the ASRCKF method can remove bad measured values. Hence, the method effectively solved the error that occurred in the measurement process and obtained accurate estimation results.

Keywords: Trajectory estimation, UWB, Adaptive, SRCKF

___

1. Introduction

The accuracy and real-time performance of trajectory estimation directly affects artillery observation and correction. The positioning technology of the sensors based on optics/acoustics [1], global positioning system (GPS) [2], and the radar [3] are often used to make trajectory estimation and improve the accuracy and real-time performance of such estimation. However, these positioning technologies have problems, such as the weak interference immunity of the sensors and the low real-time performance of the GPS. Moreover, the radar cannot overcome the influence of the low-altitude clutter waves, although it can effectively record with distinctness while playing a volley. These reasons, along with the great error in the measurement result, lead to an inaccurate ballistic estimation. Therefore, determining a strong anti-interference and real-time measurement method is important in solving the abovementioned problems.

2. State of the art

The ultra-wideband (UWB) positioning technology is a novel wireless positioning technology with high definition [4–6]. The principle of UWB is that it sends and receives significantly narrow pulses with a nanosecond or sub nanosecond scale to realize positioning. With a bandwidth of the GHz orders of magnitude, UWB positioning technology can provide accurate positioning that is precise at the decimetre level. Compared with the traditional positioning technology, UWB positioning technology has many merits, such as stability against environmental factors, strong interference immunity, short start time, small volume, easy installation, and simultaneous multi-data recording.

The positioning algorithm adopted in this paper combines the time difference of arrival (TDOA) with the angle of arrival (AOA), which are typically used in UWB positioning technology [7–9]. This algorithm can effectively improve the accuracy and coverage of the positioning and intensify the anti-destroying ability of the positioning system. However, the positioning accuracy in the process of TDOA and AOA joint positioning is still influenced by errors, such as noise. This algorithm is a nonlinear problem. Thus, nonlinear Kalman filtering method is often used to eliminate the error. The frequently-used nonlinear Kalman filter includes extended Kalman filter (EKF), unscented Kalman filter (UKF) [10], cubature Kalman filter (CKF), [11–12] and their improved algorithms.

Several filtering methods of the trajectory estimation have been analyzed and compared [13–15]. Jia B et al. adopted the high degree iteration CKF algorithm [13] and obtained high-precision positioning estimation data by comparing with EKF, UKF, and three-order CKF. However, the complexity of the result is multiplied compared with that of the three-order CKF because of the high degree of freedom. Smidl V et al. adopted the square root cubature Kalman filter (SRCKF) algorithm [14]. This algorithm avoided the non-positive definiteness problem of the

covariance and effectively improved system stability and complexity. Zhao et al. proposed the reduced twice-augmented SRCKF algorithm [15]. The algorithm augmented the noise twice in the time update and measurement update link of the cubature Kalman filter, thus effectively reducing the number of sampling points and algorithm complexity. However, in the process of UWB experiment, the result of measurement is actually not stable given a variety of unexpected reasons in the system. These bad results often bring vast errors to the system, which includes a filter fault. Thus, the current study proposed the introduction of the error covariance square root adapting factor to improve the robustness of the measurement.

The remainder of this paper is organized as follows. Section 2 expounds on the current research status of UWB positioning technology and nonlinear filtering. Section 3 presents the system model and adaptive SRCKF algorithm. Section 4 describes and analyzes the results of the simulation. Section 5 summarizes the conclusions.

3. Methodology

3.1 System modeling
This paper employed the particle trajectory model to simplify the calculation process and improve the real-time performance of the system. Figure 1 shows the constructed three-dimensional (3D) rectangular coordinate system, in which the Y axis is vertical to the ground. The coordinate of the projectile particle is (x_k, y_k, z_k), and the coordinates of the positioning base station are (x_1, y_1, z_1), $(x_2, y_2, z_2)\ldots (x_i, y_i, z_i)$. The target pitching angle and azimuthal angle measured by the positioning base station are represented by α_i and β_i, respectively.
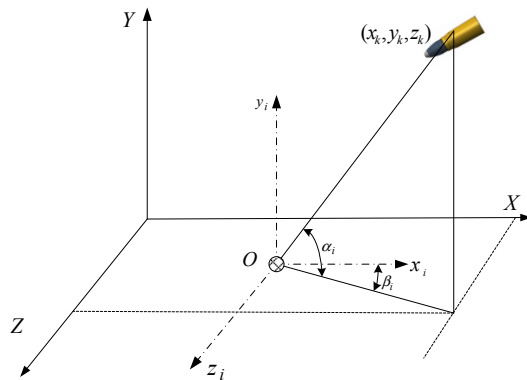
Fig. 1. TDOA/AOA Joint positioning system model diagram

3.1.1 State equation
Particle trajectory is the basis of the study of actual ballistics. Here, the projectile is a particle with the components of the location coordinate, and velocity is $[x, y, z, V_x, V_y, V_z]^T$.

Considering the wind speed, the particle trajectory equation [16] is given by

$$\begin{cases} \dfrac{dx}{dt} = v_x \\ \dfrac{dy}{dt} = v_y \\ \dfrac{dz}{dt} = v_z \\ \dfrac{dV_x}{dt} = -CH(y)G(V_r)(V_x - W_x) \\ \dfrac{dV_y}{dt} = -CH(y)G(V_r)V_y - g \\ \dfrac{dV_z}{dt} = -CH(y)G(V_r)(V_z - W_z) \end{cases} \tag{1}$$

where C is the ballistic coefficient, $H(y)$ is the air density function, $G(V_r)$ is the air resistance function, $V_r = \sqrt{(V_x - W_x)^2 + V_y^2 + (V_z - W_z)^2}$ is the relative velocity of target, W_x is the vertical wind, and W_z is the cross wind.

If $y \le 10000$ m, the air density function can be obtained according to the empirical formula [17] given by

$$H(y) = \frac{20000 - y}{20000 + y} \tag{2}$$

The air resistance function [17] is given by

$$G(V_r) = \frac{1}{2}\rho_{ON}V_r SC_{XON}(Ma) \tag{3}$$

In Formula (3), $\rho_{ON} = 1.206$ kg/m³ is the surface air density of the surface air density; C_{XON} is the standard projectile resistance coefficient, which is the function in connection with the Mach number Ma, expressed as $Ma = \dfrac{V}{C_s}$; and $C_s = \sqrt{KR_1\tau}$ is the sound velocity in which R_1 is gas constant. Substituting constants ρ_{ON} and π into Formula (3) results in

$$G(V) = 4.737 \times 10^{-4} V C_{XON}\left(\frac{V}{C_s}\right) \tag{4}$$

The ballistic coefficient and air density, in general, are regarded as constants in state equation. However, they both change in the process of the real projectile motion. Thus, they should be regarded as state variable to improve estimation precision.

The rate of the air density change is expressed as

$$\frac{d\rho}{dt} = -\rho_{ON}gV_y \tag{5}$$

The ballistic coefficient C is defined as

$$C = \frac{m}{C_D A} \tag{6}$$

where m is the mass of the projectile, C_D is the air resistance coefficient of the projectile, and A is the effective

area of the projectile. However, these three parameters cannot be used in the state equation to model the trajectory coefficient. Thus, the trajectory coefficient exponential model proposed in reference [18] was employed. The parameter β is introduced, and the resulting model of trajectory coefficient is expressed as

$$C = C_0 \exp[\beta(t)] \tag{7}$$

where C_0 is the initial value of the trajectory coefficient (experience value). The rate of β change is $\dot{\beta}(t)$ and is denoted as ω_β, which is the Gaussian white noise with zero mean.

Meanwhile, projectile location, velocity, trajectory parameters coefficient, and air density $(x, y, z, V_x, V_y, V_z, \beta, \rho)$ were chosen as the state variables. The discrete state equation is given by

$$X_{k+1} = f(X_k) + w_k = X_k + \Delta T \begin{bmatrix} V_x \\ V_y \\ V_z \\ -CH(y)G(V_r)(V_x - W_x) \\ -CH(y)G(V_r)V_y - g \\ -CH(y)G(V_r)(V_z - W_z) \\ \dot{\beta} \\ -\rho_{ON}gV_y \end{bmatrix}_{X=X_k} + w_k \tag{8}$$

where ΔT is the sampling interval. Such factors as the curvature of the earth's surface, the change of the acceleration of gravity, and Coriolis force acceleration, were not considered in the particle trajectory equation. Some errors could not be avoided. Therefore, error compensation was needed. Here, the mean of w_k is zero, and the covariance matrix is the process noise of Q_k.

3.1.2 Measurement equations
The TDOA/AOA positioning algorithm was adopted in this study, and base station 1 was set as the reference base station. The value of the system being measured included the TDOA measured value Δt_{i1} of all the base stations, except the reference base station, and the AOA measured values α_i and β_i.

(1) Measurement equation based on TDOA

$$\Delta t_{i1} = t_i - t_1 = \frac{r_i - r_1}{c} = \frac{r_{i1}}{c} \tag{9}$$

$$r_i = \sqrt{(x_i - x_k)^2 + (y_i - y_k)^2 + (z_i - z_k)^2} \tag{10}$$

$$r_{i1} = \sqrt{(x_i - x_k)^2 + (y_i - y_k)^2 + (z_i - z_k)^2} - \sqrt{(x_1 - x_k)^2 + (y_1 - y_k)^2 + (z_1 - z_k)^2} \tag{11}$$

In the above formulas, r_i is the distance from the positioning base station i to the projectile, r_{i1} is the difference between the distance from the positioning base station i to the projectile and that from the reference base station to the projectile, and c is the propagation velocity of radio wave. The measurement value was set as r_{i1}. The measurement equation was obtained based on the TDOA algorithm from Formulas (9), (10), and (11). The resulting equation is expressed as

$$Z_{k-TDOA} = \sqrt{(x_i - x_k)^2 + (y_i - y_k)^2 + (z_i - z_k)^2} - \sqrt{(x_1 - x_k)^2 + (y_1 - y_k)^2 + (z_1 - z_k)^2} + v_{k-TDOA} \tag{12}$$

where v_{k-TDOA} is the measurement noise based on the TDOA algorithm.

(2) Measurement equation based on AOA
When α_i and β_i are set as the measurement value,

$$\begin{cases} \alpha_i = \arctan \dfrac{y_k - y_i}{\sqrt{(x_k - x_i)^2 + (z_k - z_i)^2}} \\ \beta_i = \arctan \dfrac{z_k - z_i}{x_k - x_i} \end{cases} \tag{13}$$

From Formula (13), the measurement equation below can be obtained based on the AOA algorithm.

$$Z_{k-AOA} = \begin{bmatrix} \arctan \dfrac{y_k - y_i}{\sqrt{(x_k - x_i)^2 + (z_k - z_i)^2}} \\ \arctan \dfrac{z_k - z_i}{x_k - x_i} \end{bmatrix} + v_{k-AOA} \tag{14}$$

where v_{k-AOA} is the measurement noise based on the TDOA algorithm.

(3) Measurement equation based on the combination of TDOA and AOA
The value of the measurement equation based on the combination of TDOA and AOA is calculated using $z = [r_{i1}, \alpha, \beta]^T$. The measurement equation is given by

$$Z_k = h(X_k) + v_k = \begin{bmatrix} Z_{k-TDOA} \\ Z_{k-AOA} \end{bmatrix} \tag{15}$$

where $v_k = [v_{k-TDOA}, v_{k-AOA}]^T$ and v_{k-TDOA} satisfy the distribution characteristics of $N(0, e_{TDOA}^2)$, and v_{k-AOA} satisfies the distribution characteristics of $N(0, e_{AOA}^2)$. They are independent of each other, and have no relevance to x_k and w_k. Thus, the covariance of v_k is $R_k = \text{diag}(e_{TDOA}^2 I, e_{AOA}^2 I)$.

3.2 Adaptive square root cubature Kalman filter algorithm
3.2.1 Square root cubature Kalman filter
SRCKF is an improvement of the CKF ideology first proposed by Arasaratnam in 2009 [11–12], [18]. Compared with CKF, SRCKF has two advantages. First, in the process of using CKF, the non-positive definite covariance may be produced. However, SRCKF can avoid this problem effectively and improve the stability of the filter. Second, SRCKF directly uses the covariance square root matrix without further calculating the covariance. Thus, the complexity of the algorithm and filtering efficiency can be effectively reduced.

Here, the nonlinear state equation and measurement equation, such as Formula (16), were first established. SRCKF calculation was then carried out in accordance with the two steps of the SRCKF algorithm, namely, time update and measurement update.

$$\begin{cases} X_{k+1} = f(X_k) + w_k \\ Z_k = h(X_k) + v_k \end{cases} \tag{16}$$

(1) Time update
The cubature points must be structured according to the state variable dimension.

If the dimension is n, the cubature point is $\lambda_i = \sqrt{n}E$.

If $1 \leq i \leq n$, then E is a positive unit matrix with i dimensions.

If $n+1 \leq i \leq 2n$, E is a negative unit matrix with i dimensions.

If the variance estimation is $S_{k|k}$ when the time is k, the error covariance $P_{k|k}$ at this time is

$$P_{k|k} = S_{k|k}S_{k|k}{}^T \tag{17}$$

The cubature point $X_{i,k|k}$ at the time of k can be calculated by using

$$X_{i,k|k} = S_{k|k}\lambda_i + \widetilde{X}_{k|k} \tag{18}$$

The cubature point $X_{i,k+1|k}$ at the time of $k+1$ that was deduced from the cubature point $X_{i,k|k}$ is

$$X'_{i,k+1|k} = f(X_{i,k|k}, U_k) \tag{19}$$

The predictive value of state $\widetilde{X}_{k+1|k}$ at the time of $k+1$ is given by

$$\widetilde{X}_{k+1|k} = \frac{1}{2n} \sum_{i+1}^{2n} X'_{i,k+1|k} \tag{20}$$

The predictive value of error covariance square root $S_{k+1|k}$ is stated as

$$S_{k+1|k} = Tria\left(\left[X'_{i,k+1|k}, S_{Q,k}\right]\right) \tag{21}$$

where $S_{Q,k}$ is the square root of Q_k, and $Q_k = S_{Q,k}S_{Q,k}^T$.

The weighted center matrix $X'_{k+1|k}$ is given by

$$X'_{k+1|k} = \frac{1}{2n}\begin{bmatrix} X'_{1,k+1|k} - \widetilde{X}_{k+1|k}, X'_{2,k+1|k} \\ -\widetilde{X}_{k+1|k}, \cdots, X'_{2n,k+1|k} - \widetilde{X}_{k+1|k} \end{bmatrix} \tag{22}$$

(2) Measurement update
An equation is used to calculate the updated cubature point $X_{i,k+1|k}$. The equation is given by

$$X_{i,k+1|k} = S_{k+1|k}\lambda_i + \widetilde{X}_{k+1|k} \tag{23}$$

The predictive value of measurement cubature point $Z_{i,k+1|k}$ at the time of, which is calculated via measurement equation, is given by

$$Z_{i,k+1|k} = h(Z_{i,k+1|k+1}, U_k) \tag{24}$$

The measurement estimate $\widetilde{Z}_{k+1|k}$ is expressed as

$$\widetilde{Z}_{k+1|k} = \frac{1}{2n} \sum_{i+1}^{2n} Z_{i,k+1|k} \tag{25}$$

The value of innovation covariance square root $S_{ZZ,k+1|k}$ is given by

$$S_{ZZ,k+1|k} = Tria\left(\left[Z_{i,k+1|k}, S_{R,k+1}\right]\right) \tag{26}$$

where $S_{R,k+1}$ is the square root of R_{k+1}, and $R_{k+1} = S_{R,k+1}S_{R,k+1}^T$.

The weighted center matrix $Z_{k+1|k}$ is calculated using

$$Z_{k+1|k} = \frac{1}{2n}\begin{bmatrix} Z_{1,k+1|k} - \widetilde{Z}_{k+1|k}, Z_{2,k+1|k} \\ -\widetilde{Z}_{k+1|k}, \cdots, Z_{2n,k+1|k} - \widetilde{Z}_{k+1|k} \end{bmatrix} \tag{27}$$

The values of innovation covariance $P_{ZZ,k+1|k}$ and measurement auto-covariance $P_{Z,k+1|k}$ are

$$\begin{cases} P_{ZZ,k+1|k} = S_{ZZ,k+1|k}P_{ZZ,k+1|k}^T \\ P_{Z,k+1|k} = P_{ZZ,k+1|k} - R_{k+1} \end{cases} \tag{28}$$

The cross-covariance of the predictive value of state and measurement estimation $P_{XZ,k+1|k}$ is given by

$$P_{XZ,k+1|k} = X_{k+1|k}Z_{k+1|k}^T \tag{29}$$

where $X_{k+1|k}$ is

$$X_{k+1|k} = \frac{1}{2n}\begin{bmatrix} X_{1,k+1|k} - \widetilde{X}_{k+1|k}, X_{2,k+1|k} \\ -\widetilde{X}_{k+1|k}, \cdots, X_{2n,k+1|k} - \widetilde{X}_{k+1|k} \end{bmatrix} \tag{30}$$

The filter gain $K_{k+1|k}$, state estimation $\widetilde{X}_{k+1|k+1}$, and estimation error covariance square root $S_{k+1|k+1}$ are expressed as

$$\begin{cases} K_{k+1|k} = \left(P_{ZZ,k+1|k} / S_{ZZ,k+1|k}^T\right)/S_{ZZ,k+1|k} \\ \widetilde{X}_{k+1|k+1} = \widetilde{X}_{k+1|k} + K_{k+1|k}\left(Z_{k+1|k+1} - \widetilde{Z}_{k+1|k}\right) \\ S_{k+1|k+1} = Tria\left(\left[X_{k+1|k} - K_{k+1|k} \times Z_{k+1|k}, K_{k+1|k}S_{R,k+1}\right]\right) \end{cases} \tag{31}$$

3.2.2 Adaptive square root cubature Kalman filter
(1) Adaptive principle

The SRCKF algorithm is quite sensitive to the change of measurement conditions. Given a variety of unexpected problems in using UWB technology, the result of measurement is not stable and may produce some undesirable values (Figure 2). These values would easily lead to filter instability and even filter divergence. Thus, the matching of the real and estimated values of the innovation covariance square roots is used to determine the accuracy of the measurement, eliminate the undesirable values, and implement the adaptability of system. In turn, these can improve the system robustness in the measurement process.
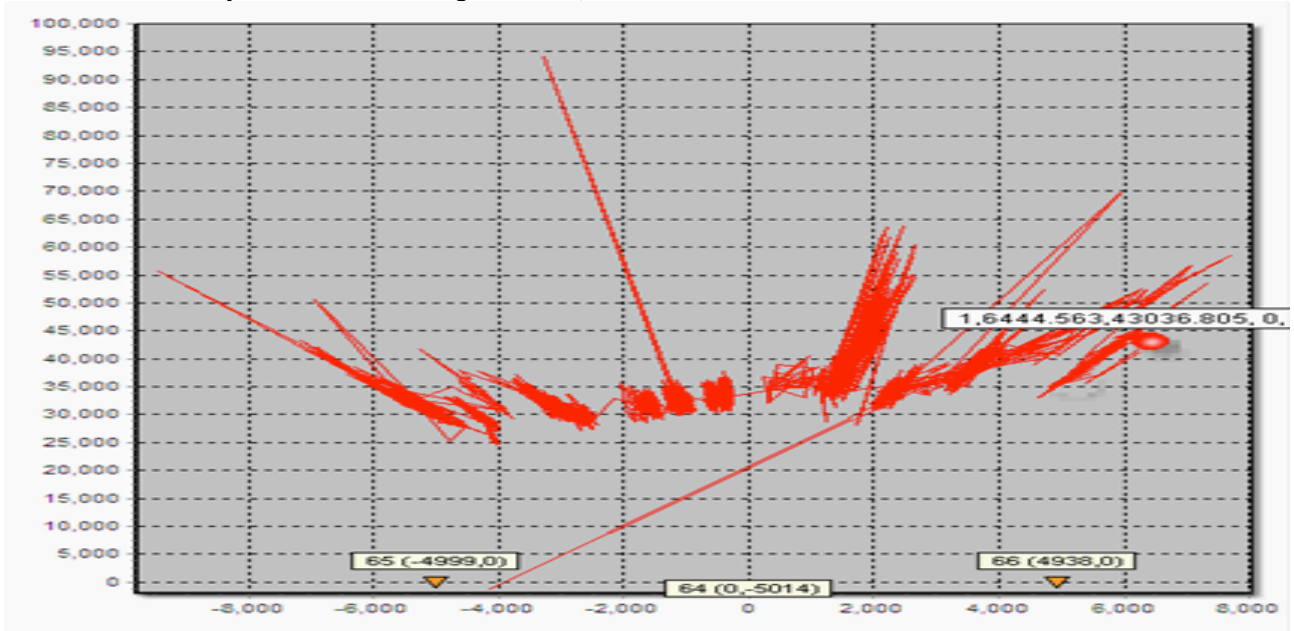
Fig. 2. The measurement trajectory of the UWB dynamic detection target hovering at 300 m

(2) Adaptive application in the SRCKF
The filter innovation is given by

$$\mu_{k+1} = Z_{k+1} - \tilde{Z}_{k+1|k} \tag{32}$$

The adaptive factor ρ_{k+1} is introduced.

If there is no undesirable value, $S_{ZZ,k+1|k}$ and $S_{k+1|k+1}$ are shown in Formulas (26) and (31), respectively.

Otherwise, Formulas (26) and (31) need to introduce the adaptive factor ρ_{k+1} expressed as

$$\begin{cases} S_{ZZ,k+1|k} = Tria\big([Z_{i,k+1|k}, \rho_{k+1}S_{R,k+1}]\big) \\ S_{k+1|k+1} = Tria\big([X_{k+1|k} - K_{k+1|k} \times Z_{k+1|k}, K_{k+1|k}\rho_{k+1}S_{R,k+1}]\big) \end{cases} \tag{33}$$

Formula (33) can effectively avoid the undesirable value obtained in the iterative process during the measurement and ensure the stability of the filter.

The adaptive factor ρ_{k+1} is calculated as

$$\begin{cases} \mu_{k+1}\mu_{k+1}^T = P_{ZZ,k+1|k} \\ P_{ZZ,k+1|k} = P_{Z,k+1|k} - \rho_{k+1}^2 R_{k+1} \\ \mu_{k+1}\mu_{k+1}^T = tr\big[\mu_{k+1}\mu_{k+1}^T\big] \end{cases} \tag{34}$$

The following is obtained with Equation (35):

$$tr\big[\mu_{k+1}\mu_{k+1}^T\big] = tr\big[P_{Z,k+1|k} - \rho_{k+1}^2 R_{k+1}\big] \tag{35}$$

Consequently, the adaptive factor ρ_{k+1} could be obtained by using

$$\rho_{k+1} = sqrt\left(\frac{\mu_{k+1}\mu_{k+1}^T - tr\big[P_{Z,k+1|k}\big]}{tr\big[R_{k+1}\big]}\right) \tag{36}$$

(3) Application of the adaptive algorithm
The measurement results are tested using the statistical function expressed as

$$\zeta_{k+1} = \mu_{k+1}\big[P_{ZZ,k+1|k}\big]^{-1}\mu_{k+1}^T \tag{37}$$

where ζ_{k+1} obeys the χ^2 distribution with the freedom of n (vector dimensions). If the precision of the measurement result must be controlled within the range of ε $(0 < \varepsilon < 1)$, then

$$P\big(\chi^2 > \chi_{\varepsilon,M}^2\big) = \varepsilon \tag{38}$$

Formula (38) shows that $\chi_{\varepsilon,M}^2$ is the measurement threshold. If $\zeta_k > \chi_{\varepsilon,M}^2$, the adaptive factor must be calculated to correct the value of innovation covariance square root that participated in the measurement update process.
Selection process:
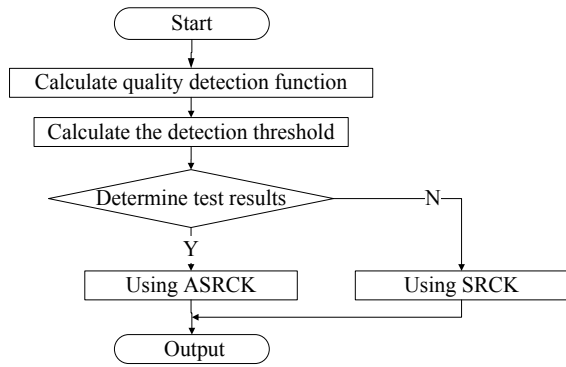
Fig. 3. The selection process of the adaptive algorithm

The processes described in Formulas (16) to (38) show the state equation and measurement equation of the trajectory. Adaptive square root cubature Kalman trajectory estimation can be implemented based on the combination of AOA and TDOA.

4 Results and discussion

A UWB tag was installed in the bullet (Figure 4), and the base station was set in the range. The exeperiment was completed by computer simulation when experimental conditions cannot be simulated.
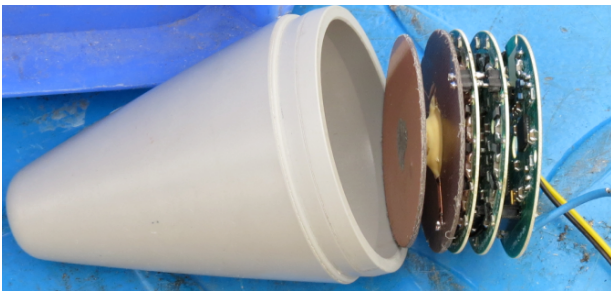
Fig. 4. The experiment projectile with the UWB tag

4.1 Performance comparison of TDOA/AOA and TDOA
The effectiveness analysis of the TDOA/AOA joint positioning algorithm mentioned above was carried out by computer simulation. The initial value of state variable $X = [x, y, z, V_x, V_y, V_z]^T$ was set as $X_0 = [10000, 0, 80, -879, 190, -12]^T$. Using TDOA/AOA joint measurement requires at least three base stations. Three base stations were adopted to simplify the calculation. The three base stations were the two positioning base stations of AOA with the coordinates of $BS_1(50,0,0)$ and $BS_2(-50,0,0)$ and the positioning base station measuring AOA with the coordinate of $BS_3(0,0,0)$, respectively. At least three base stations were needed in using TDOA/AOA joint measurement, whereas using TDOA measurement required at least four base stations. This paper adopted four base stations to simplify the calculation, and the coordinates were $BS_1(0,0,0)$, $BS_2(50,0,0)$, $BS_3(-50,0,0)$, and $BS_4(0,0,-50)$, respectively, with BS_1 serving as the reference base station. The measurement standard deviation was 100 m, the sampling interval was 0.25 s and both the vertical wind W_x and cross wind W_z were 10 m/s. The

measurement trajectory before the measurement results are treated is shown in Figure 5.
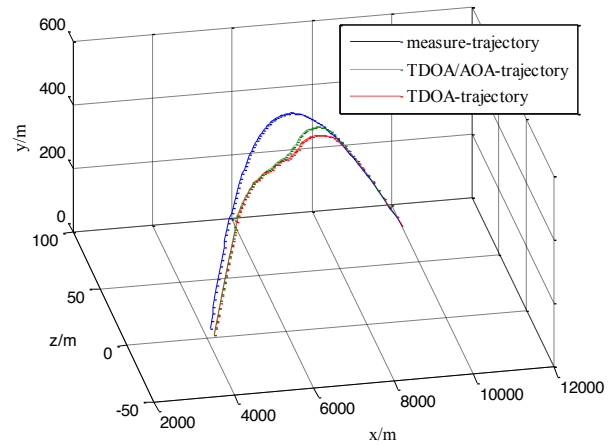
Fig. 5. Ballistic-trajectory and measurement-trajectory

SRCKF was used to conduct the filter estimation of the two kinds of measurement results. The measurement noise standard deviations of TDOA and the combination of TDOA/AOA were $\sigma_r = 100$ m and $\sigma_r = 100$ m, respectively. The impact of the measurement accuracy of AOA on the measurement results of TDOA/AOA was analyzed by changing the value of the measurement noise standard deviation of AOA into 1°, 2°, 3°, and 4°. The results were then compared with the measurement results of TDOA to analyze the performances of both approaches.

The root mean square error (RMSE) was taken as the standard by which to measure the estimation accuracy. This is calculated using

$$RMSE_x(k) = \sqrt{\frac{1}{N} \sum_{i=1}^{N} (x_i(k) - \hat{x}_i(k))^2} \tag{39}$$

where N is the number of simulation time, and $x_i(k)$ and $\hat{x}_i(k)$ are the real value and the estimated value of the state vector, respectively, which helped obtain the value of $N(i)$ and time (k).

About 200 Monte-Carlo simulations were implemented based on the initial conditions and parameters. The curves of the position RMSE of the TDOA and TDOA/AOA are shown in Figure 6.
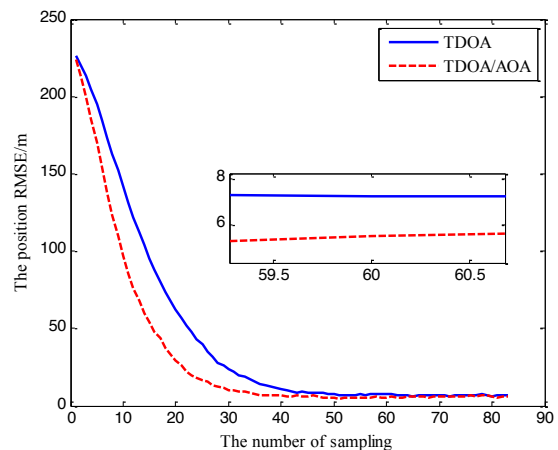
(a) The standard deviation of AOA is 1°
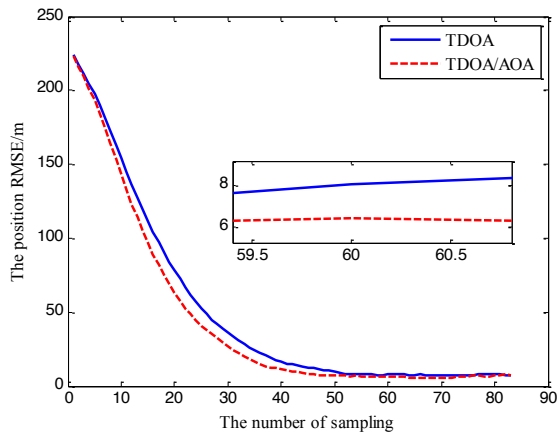
(b) The standard deviation of AOA is 2°
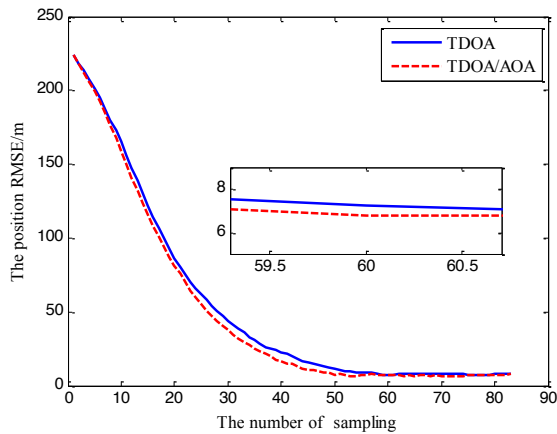
(c) The standard deviation of AOA is 3°
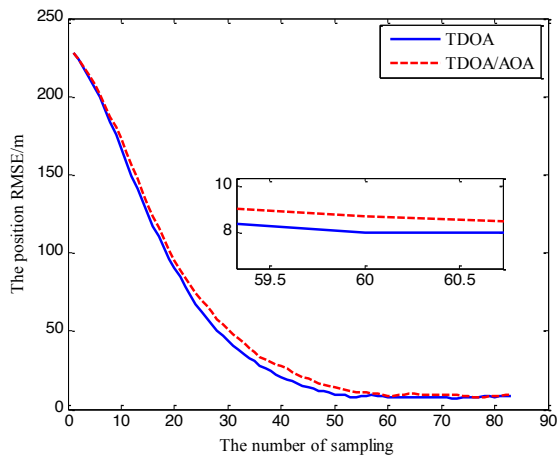
(d) The standard deviation of AOA is 4°

Fig. 6. The position RMSEs of TDOA and TDOA/AOA under different standard deviation values of AOA

The mean values of the results are shown in Table 1.

Table 1. Comparison of the position RMSE mean values of TDOA and TDOA/AOA under different standard deviation values of AOA

Standard deviation of AOA /°	1°	2°	3°	4°
Measurement point error of TDOA /m	44.13	50.03	54.31	54.82
Measurement point error of TDOA/AOA/m	31.83	44.37	50.69	58.64
Precision variation	↑27.82%	↑11.31%	↑6.67%	↓6.97%

As shown in Table 1, if the standard deviation of AOA was controlled in a certain range, the performance of the measurement method based on the combination of TDOA/AOA would be better than that based on TDOA only. Moreover, the measurement method based on the combination of TDOA/AOA gradually lost its majority along with the increase of the standard deviation of AOA. The standard deviation of AOA fell out of that range. Moreover, the performance of the measurement method based on TDOA was improved compared with that based on the combination of TDOA/AOA.

4.2 ASRCKF performance simulation
ASRCKF performance simulation was carried out based on the TDOA/AOA measurement process. The initial state, base station layout, sampling interval, states noise, and wind conditions were the same as those in Section 3.1. Moreover, $\sigma_r = 100$ m and $\sigma_\alpha = \sigma_\beta = 1°$.

4.2.1 Effect of the undesirable measurement value on the filter performance
The main function of ASRCKF was to eliminate the undesirable values obtained during the measurement process. A forward mutation x=500 m was added into the simulation test when k=40 to compare the performances of ASRCKF and SRCKF. The filtering curve on the x direction is shown in Figure 7.
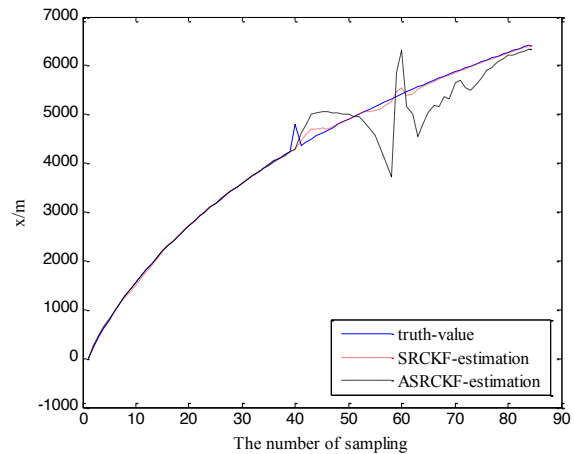
Fig. 7. The estimated curves of SRCKF and ASRCKF accompanied by undesirable values

As shown in Figure 7, SRCKF estimation diverged when the undesirable values emerged. The error remained significantly large even though there was a trend of convergence. The ASRCKF estimation curve fluctuated slightly and had rapid convergence speed. Thus, its stability was significantly higher than that of SRCKF. The RMSEs of SRCKF and ASRCKF in the x direction are shown in Table 2.

Table 2. The RMSEs of SRCKF and ASRCKF in the x direction

Filter method	SRCKF	ASRCKF
RMSE/m	383.86	74.43

4.2.2 Effect of the noise mutation on filter performance
The statistical characteristic of noise was uncertain in the filtering process. In order to examine the effect of the noise mutation on the ASRCKF algorithm, $\sigma_r = 100m$ was changed to $\sigma_r = 900m$ when k=40 during simulation. The

RMSE curves of SRCKF and ASRCKF are shown in Figure 8.
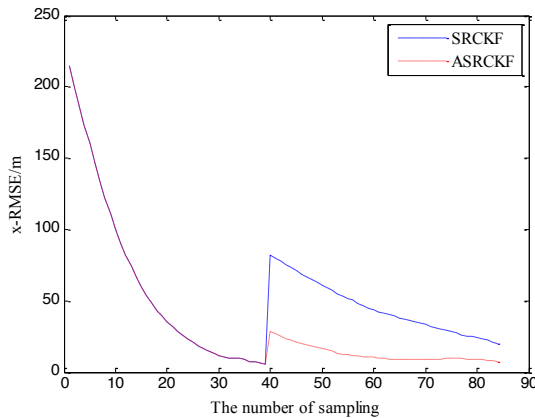
Fig. 8. The RMSE curves of SRCKF and ASRCKF under measurement noise mutation

Based on the comparison of SRCKF and ASRCKF in Figure 8, once the noise statistics changed in the process of filtering, the RMSE of SRCKF increased tremendously and did not converge rapidly again. Meanwhile, under the measurement noise mutation, the RMSE of ASRCKF with its own adaptive ability was less affected and can quickly converge to the real value of the system state.

5. Conclusions

In view of the bad anti-interference performance of the current ballistic measurement method, this study used UWB as the ballistic measurement method. ASRCKF was proposed to eliminate the bad values in the measurement process. ASRCKF was also used in matching the real and estimate values of the innovation covariance square roots to determine the accuracy of the measurement. The following conclusions can be drawn from the system simulation.

(1) If the standard deviation of AOA was controlled in a certain range, the performance of the measurement method based on the combination of TDOA/AOA proved to be better than that based on TDOA only.

(2) When undesirable values occurred or when the noise statistical characteristics became inaccurate, the RMSE of ASRCKF with its own adaptive ability was less affected and quickly converged to the real value of the system state compared with SRCKF.

The findings of this study can help improve the accuracy of trajectory estimation and provide more accurate bases for ballistic correction. However, the algorithm is limited by some problems, such as long sampling time and device synchronization. Thus, further studies are needed to solve the aforementioned problems.

References

1. Zhang H (2014). *Tracking Techniques for Midcourse Target Complex via Space-based Infrared Sensors* (Doctoral dissertation). Retrieved from http://www.cnki.net/KCMS/detail/detail.aspx
2. Yang X H, Huo P F, Wang C. "GPS Trajectory Measurement Errors Elimination Based on Kalman Filtering", *Journal of Detection&Control* , 34(4), 2012, pp. 30-33.
3. Wesson K, Shepard D, Humphreys T. "Straight talk on anti-spoofing: securing the future of PNT", *GPS World*, 23(1), 2012, pp. 32-39.
4. Win M, Conti A, Mazuelas S. "Network localization and navigation via cooperation", *IEEE Communications Magazine*, 49(5), 2011, pp. 56-62.
5. Steiner C, Wittneben A. "Low complexity location fingerprinting with generalized UWB energy detection receivers", *IEEE Transactions on Signal Processing*, 58(3), 2010, pp. 1756-1767.
6. Zhou Yuan, Law C, Guan Y L. "Indoor elliptical localization based on asynchronous UWB rang measurement", *IEEE Transactions on Instrumentation and Measurement*, 60(1) , 2011, pp. 248-257.
7. Taponecco L, D'Amico A, Mengali U. "Joint TOA and AOA estimation for UWB localization applications", *IEEE Transactions on Wireless Communications*, 10(7), 2011, pp. 2207-2217.
8. Lin L X, So H C, Chan K W. "A new constrained weighted least squares algorithm for TDOA-based localization", *Signal Processing*, 93(10), 2013, pp. 2872-2878.
9. Brutti A, Nesta F. "Tracking of multidimensional TDOA for multiple sources with distributed microphone pairs", *Computer Speech and Language*, 27(3), 2013, pp. 660-682.
10. Julier S, Uhlmann J, Durant-Whyte H F. "A new method for the nonlinear transformation of mean and covariances in filters and estimators", *IEEE Transactions on Automatic Control*, 45(3), 2000, pp.477-482.
11. Ienkaran Arasaratnam, Simon Haykin. "Cubature Kalman Filters", *IEEE Transaction on Automatic Control*, 56(6), 2009, pp.1254-1269.
12. Ienkaran Arasaratnam, Simon Haykin, Thomas R Hurd. "Cubature Kalman Filters for Continuous-Discrele System:Theory and Simulations", *IEEE Transaction on Signal Processing*, 58(10), 2010, pp.4977-4993.
13. Jia B, Xin M, Cheng Y. "High-degree cubature kalman filters", *Automatica*, 49, 2013, pp. 510-518.
14. Smidl V, Peroutka Z. "Advantages of square-root extended kalman filter for sensorless control of AC drives", *IEEE Transactions on Industrial Electronics*, 59(11), 2012, pp.4189-4196.
15. Zhao X J, Wang L X, He Z K. "Reduced twice augmented square root cubature Kalman filter and its application", *Acta Aeronauticae Astronautica Sinica*, 35(8) , 2014, pp. 2286-2298.
16. Ghosh S, Mukhopadhyay S. "Tracking reentry ballistic targgets using acceleration and jerk models", *IEEE Transactions on Aerospace and Electronic System*, 47(1), 2011, pp. 666-683.
17. Kim T H, Moon K R, Song T L. "Variable-structured interacting multiple model algorithm for the ballistic coefficient estimation of a re-entry ballistic target", *International Journal of Control, Automation and Systems*, 11(6) , 2013, pp.1204-1213.
18. Li X R, JiKov V P. "Survey of maneuvering target tracking (Part II): Motion Models of Ballistic and space Targets", *IEEE Trans.on Aerospace and Electronic Systems*, 46(1), 2010, pp. 96-119.